

OTC-26668-MS

Consistent Design Criteria for South China Sea with a Large-Scale Extreme Value Model

L. Raghupathi, Shell India Markets Pvt. Ltd.
D. Randell, P. Jonathan; Shell Global Solutions (UK)
K.C. Ewans, Sarawak Shell Bhd.

Abstract

Existing metocean design criteria for offshore facilities in the South China Sea have been estimated using different data and procedures, some of which are at least partly *ad hoc*. As a result, it is probable that existing criteria are inconsistent, in the sense that assets designed to the same design codes have different realised levels of integrity. To address this concern in this paper, we apply a large-scale extreme value model adapted to parallel computing environment, applied to the recent high-resolution SEAFINE hindcast database. This not only ensures design criteria that are statistically and spatially consistent but is also faster by avoiding the need for repetitive site-specific analysis.

We have to overcome several challenges before we can apply a large-scale extreme model on the SEAFINE database. These include identifying a spatially consistent set of storm peaks and validating the hindcast data with real measurements. We then estimate marginal return values for significant wave height for locations within a large spatial neighbourhood, accounting for spatial and storm directional variability of peaks over threshold. A quantile regression identifies the extreme value threshold, the rate of exceedance of which is described using a Poisson process. The size of threshold exceedances is described by a generalised Pareto model. The characteristics of the threshold, rate and size models are all non-stationary with respect to directional and spatial covariates, parameterised in terms of (multi-dimensional) penalised B-splines. Parameter estimation is computationally challenging, but a combination of efficient generalised linear array algorithms executed within a parallel computing environment enable maximum likelihood estimation of all models. Bootstrap resampling is used to estimate uncertainties of model parameters and return values.

We thus estimate consistent marginal return values for significant wave height and their uncertainties, at all locations in the spatial neighbourhood. In addition, we quantify directional variability of return values across different return periods. We rigorously validate the proposed spatio-directional model with that of a direction-only model by deriving model diagnostics for the same site and demonstrating equivalent goodness of fits. To our knowledge this is the first of a kind of application of large-scale estimation for the South China Sea. With this approach, design criteria for large spatial domains, non-stationary with respect to the appropriate environmental covariates, can be estimated efficiently, consistently and with quantified uncertainty.

1. Introduction

1.1 Background

Safe and reliable design and operation of fixed and floating marine structures often located in remote and hostile environments is challenging. This requires the design and construction of structures able to withstand severe environmental conditions, more extreme than the worst foreseeable during the required structural lifetime, associated with an annual probability of failure typically less than 1 in 10,000. Rigorous extreme value analysis of meteorological and oceanographic (or *metocean*) data can greatly aid the design of such structures. Robust modelling of extreme environmental conditions is therefore critical for safe day-to-day operation and long-term structural reliability. A recent review is presented in Jonathan and Ewans (2013).

The existing metocean design criteria for offshore facilities in the South China Sea (SCS) have been estimated using different data and procedures, some of which are at least partly *ad hoc*. Conventionally, only data corresponding to one location of interest, or a pool of neighbouring locations, are used to estimate site-specific design criteria. This could be due to the lack of a spatial grid at sufficient resolution and also because of the lack of an extreme value approach to effectively model spatial covariate effects. As a result, it is probable that existing criteria are inconsistent, in the sense that assets designed to the same design codes have different realised levels of integrity. To address this concern, in this work, our objective is to provide design criteria that are statistically and spatially consistent.

We aim to extend our previous work on whole-basin extreme value analysis to the SEAFINE hindcast database. SEAFINE (SEAMOS-South Fine Grid Hindcast) is an Oceanweather JIP (Joint Industry Project) for development of wind and wave hindcast data on a fine grid of the southern part of the SCS (Oceanweather, 2014). SEAFINE is based on a uniform 25-km grid embedded with very-high resolution fine grid nests each with grid spacing of about 6 km. The hindcast covers a continuous period 1956-2012, which is considerably longer than what was available earlier. Thus, with the improved hindcast model available at higher resolution than earlier, we expect to have a more elaborate and rigorous set of historical data input, required for better estimation of design criteria.

1.2 Challenges

Our earlier work (Raghupathi et al., 2016c) made whole-basin marginal modelling (i.e., to estimate independent design criteria of winds, waves, etc.) possible for spatio-directional problems by developing efficient statistical algorithms and then adapting them to parallel computing environments. We estimated the marginal return values for significant wave height (H_s) for locations in the Gulf of Mexico (GoM) within a large spatial neighbourhood, accounting for spatial and storm directional variability of peaks over threshold. However, it is not straightforward to apply this method to the SCS.

There are several challenges in extending our approach to the SCS. First, for the earlier analysis done for the GoM, the hindcast database (known as GOMOS) includes specific information on tropical and extra-tropical hurricanes, especially the starting and ending periods (Oceanweather, 2008). During the preparation of the hindcast database, experienced oceanographers, using specialist tools, carefully went through a multitude of data sources to precisely decipher storm tracks and intervals. These include in-situ data such as ocean buoys, ship reports and coastal observations and remote ones such as satellites, aircraft and radar, storm reports from NOAA/NHC, etc. Thus, once this information is made available, it is relatively straightforward to identify the peak events within the specified intervals for the entire basin. However, the latest hindcast for the SCS (known as SEAFINE details of which are given in §2) being a continuous-time hindcast, no such information is available. Also the SCS meteorology consists of both monsoons and typhoons and hence does not contain “well-defined” storm periods. To accomplish this,

we need to generate a consistent set of “storm peaks” over a given spatial domain to perform large scale extreme value analysis. The consistent identification of peaks has been discussed in detail in Raghupathi et al. (2016a). In this work, we apply this spatial peaks identification for generating consistent design criteria.

Second, SEAFINE is a relatively new database covering a region with significant local variations (due to bathymetry, change in wind fields due to the presence small islands, etc.) which has not been validated by comparing with the available platform measurements. Thus, we have also developed approaches to validate the hindcast before applying the extreme value model.

Third, unlike the GoM where extreme design criteria is driven primarily due a single physical phenomenon i.e., hurricanes, the SCS exhibits heterogeneous behaviour with strong seasonal variations. SCS regional climate is characterised by northeast and southwest monsoons coupled with the effects of passing typhoons. Statistical modelling of these directional and seasonal effects over a spatial domain is much more challenging.

Figure 1 illustrates the overall workflow of our proposed approach. We start with the raw hindcast data (SEAFINE in this case), validate it using known platform measurements. For the set of interested grid locations, we then apply the spatial peak picking algorithm for identifying spatially consistent storm peaks. We then apply the **Spatial Covariate Extreme Value Analysis** or **SCEVA** on the set of storm peaks thus identified. The above steps can be applied to any metocean parameter (H_s , W_s , etc.) for any given set of locations. This produces consistent design criteria for the locations of interest.

Though the scope of the current work is the SCS, the methods described herein are generic to be applied to any ocean basin for which a historical hindcast database is available. The rest of this paper is organised as follows. §2 explains the regional meteorology of the SCS region in brief, and describes the SEAFINE hindcast data used in this study and the methods used to validate these data with actual platform measurements. §3 describes the extreme value modelling steps used to analyse the SEAFINE and estimate the model parameters. Finally, §4 illustrates the results of the model by providing appropriate model diagnostics and generating spatially consistent design criteria for a set of spatial grid locations in the SCS, followed by discussion in §5.



Figure 1. Flowchart illustrating the proposed workflow of generating consistent regional criteria using the *Spatial Covariate Extreme Value Analysis* (SCEVA) approach.

2. Data Preparation and Validation

In this section, we describe the SEAFINE database in greater detail, the steps undertaken to validate the data with the available measurements and briefly the peak picking step required to apply the large-scale extremes model.

2.1. South China Sea: Metocean Conditions

The northeast and southwest monsoons and the effects of the occasional passing typhoon characterise the climate offshore Northwest Borneo (Borneo, 2015).

NE Monsoon (November to March) characterised by predominantly north-east winds, increased cloudiness and the heaviest rainfall of the year. Regular surges in the monsoon increase winds and local waves, and the height of the swell breaking on the beaches of NW Borneo.

Transition (April - May) when the winds are light (except during occasional squalls) and variable in direction.

SW Monsoon (June to September) with predominantly southwest winds is normally quieter than the NE Monsoon but is also characterised by surges and periods of unsettled weather. The SW monsoon surges are often associated with typhoons passing to the north of Borneo.

Transition (October/November) sees changeable wind direction with an increase in wind speed and frequency of squalls. It is also the time of the year when the risk of typhoons affecting the area is greatest. The number of typhoons crossing the Philippine Islands from the western Pacific into the northern part of the SCS averages around 20 per year. These typhoons generally move in a west-north westerly direction, bounded by the latitudes 10 to 20 degrees North, and pass into China or Vietnam. Very occasionally, typhoons form further south in the Sulu Sea or offshore Sabah and these track westwards into the Gulf of Thailand.

2.2. SEAFINE Hindcast Database

The joint-industry project SEAMOS (South East Asia Meteorological and Oceanographic Hindcast Study) was the first study to provide definitive data on meteorological and oceanographic extreme and operational conditions, to be used in aid of design of offshore structures and planning of offshore operations in the general area of the SCS. The wave field over the SCS is hindcast using a directional spectral model which resolves the study domain on a grid of 25 km spacing. A depth integrated storm surge and current model was used to develop storm-generated water levels and flow velocities in the historical storms. The surge and current hindcast was continuous, using surface wind and wave fields at 50-km resolution over the 10-year period 1980-1989 (Oceanweather, 1992).

The complexity of the bathymetry and the relative sparseness of tropical cyclones in these parts of the basin present some special problems that are addressed in this SEAMOS follow-up project dubbed SEAFINE (SEAMOS South Fine Grid Hindcast). SEAFINE not only provides an updated and greatly expanded (in terms of the historical period addressed) treatment of the entire southern half of the SEAMOS domain but also very high-resolution metocean hindcast carried out with fine mesh nested grids covering the offshore and coastal resource development areas of interest to the participants of SEAFINE. The SEAFINE hindcast database comprises of 56 years of historical metocean data for a large spatial domain available at fine grid resolution of 0.05° to 0.25° (Oceanweather, 2014).

Figure 2 shows the spatial extent of the SEAMOS and SEAFINE grids. For the shallow water blocks (say offshore Borneo), the SEAFINE data are available at a resolution much higher (up to 5 times) than earlier. This, along with the extended period of data (again more than 5 times), means that the SEAFINE has a higher quality of input data that is very important to derive robust extreme value statistics. This, when used on an extreme value model with spatial covariates may therefore result in an improved estimation of design criteria that are spatially consistent. However, in order to accomplish this we need to overcome the technical challenges mentioned in §1.2 using solutions that will be described next.

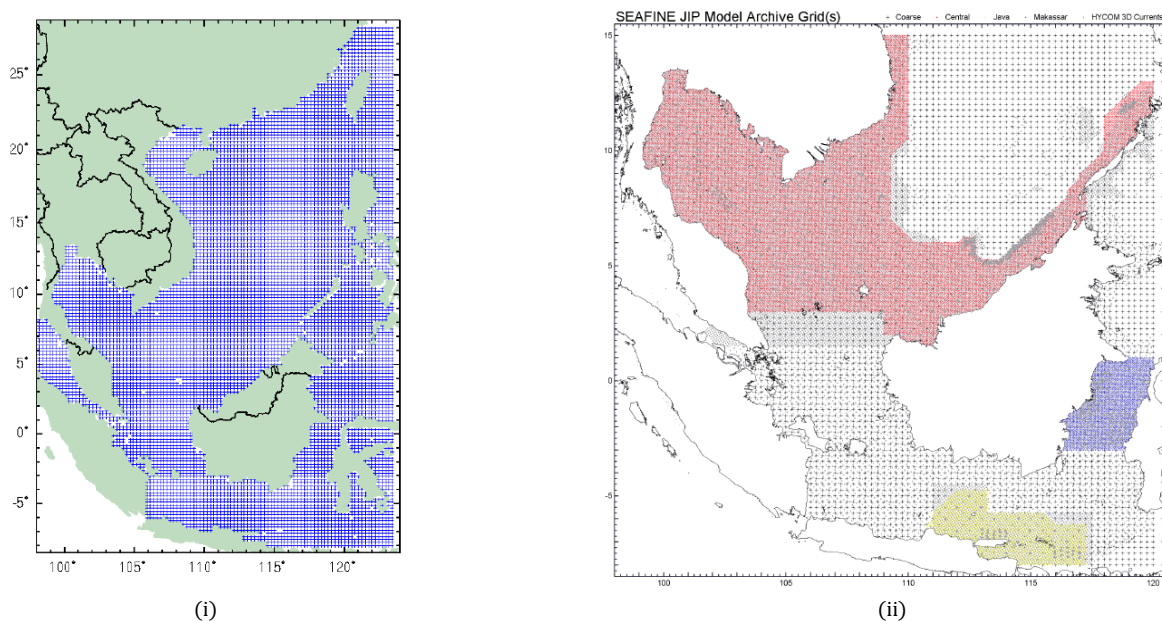


Figure 2. (i) Grid locations of the coarser SEAMOS hindcast database. (ii) Grid locations of the SEAFINE hindcast database. (Image courtesy: Oceanweather Inc.)

2.3. Spatial Peak Picking: Application to SEAFINE

Our motivation is to extend our previous basin-wide extremes modelling to other ocean basins in general and the SCS in particular. To accomplish this, we need to generate a consistent set of “storm peaks” over a given spatial domain to perform large scale extreme value analysis. As summarised under the challenges in §1, the hindcast data for the GoM includes specific information on tropical and extra-tropical hurricanes, especially the starting and ending periods.

However, SEAFINE being a continuous-time hindcast, no such information is available. Also the SCS meteorology consists of both monsoons and typhoons and hence does not contain “well-defined” storm periods. The monsoon surge can come both due to monsoons (on a much larger time and spatial range) and due to typhoons (which intensely target a given location during a particular period). Our approach to tackle this problem is based on careful study of the storm peak events over a given spatial domain. Techniques have been developed to propagate these peaks over space, consolidate them if they represent the same storm event, and to finally put together the metocean parameters of interest over the entire spatial domain of interest. In addition, diagnostic tools have been developed in order to choose the right set of input parameters to generate a consistent set of peaks over a given spatial domain. Further details are provided in Raghupathi et al. (2016a).

We now present results of applying the spatial peak picking on the H_s for the given set of grid locations in Figure 3. Each plot shows the raw time series (black line) and the peaks detected (blue diamonds) for a set of 9 sites of interest in the SCS. The start and end of each peak period is show using green and red

('x') marks respectively. The left plots show the peak picking step done *independently* for each site. We observe that each site obviously has different number of peaks detected as one would expect (indicated by the plot title). The right plots show the results of propagation and consolidation across these 9 sites. We observe here that each site has the same number of peaks detected. Parameters for an appropriate choice of threshold and merging interval were chosen after careful analysis of diagnostic plots. We observe that many of the smaller peaks have been merged into one big peak with a large storm period. Also notice that in certain case (see the right most peak), the peaks occur at different times within the super interval created after consolidation though representing the same storm event.

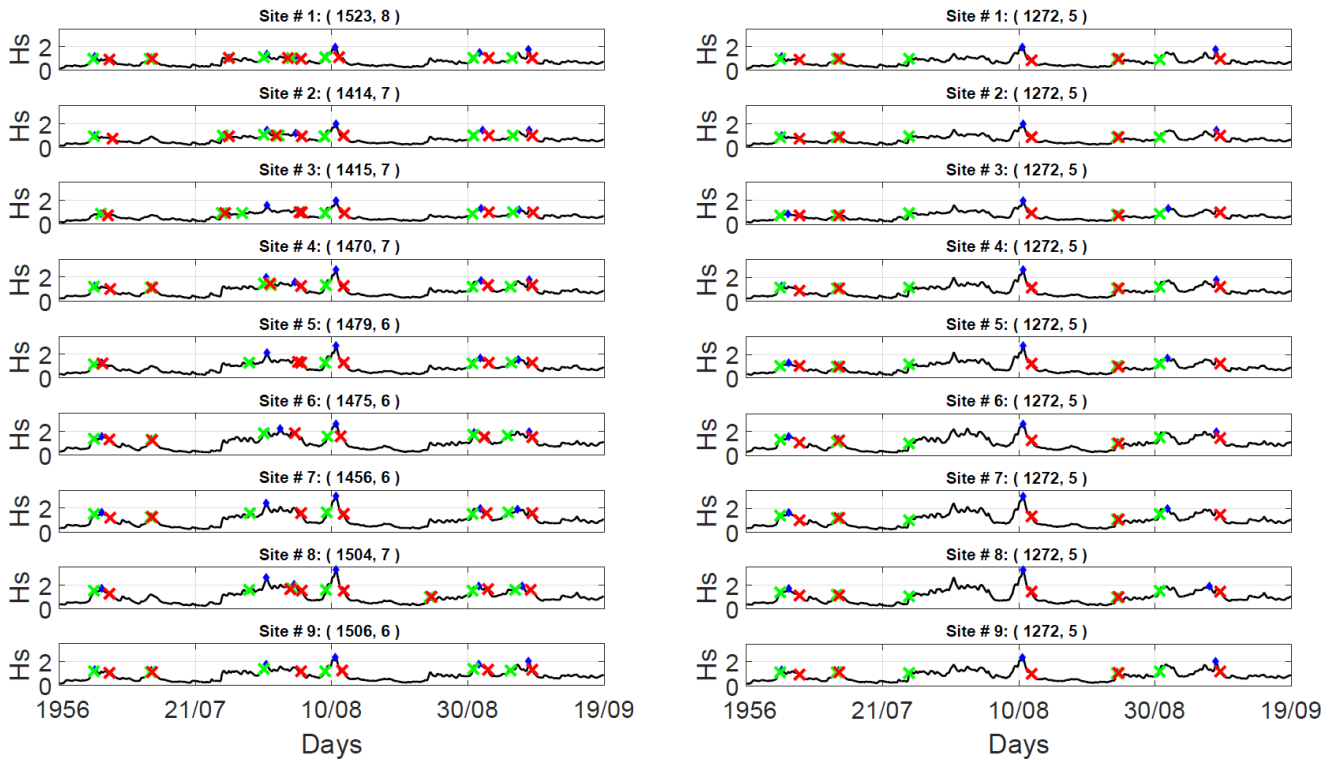


Figure 3. Spatial peak picking illustrated for a set of locations in the SCS showing the initial independent peaks (left) and after the spatial consolidation step (right). In each plot, the time series is shown in black and the peaks indicated by blue diamonds and the start and end of each peak period is show using green and red ('x') marks respectively. The title in parenthesis indicates the number of peaks detected overall for the entire 56-year period and within this time window.

2.4. Validation of SEAFINE Hindcast

For deriving extreme statistics, we often rely on hindcast models due to the availability of high resolution data for long periods. Even when platform measurements are available for comparative periods, they often have missing periods, measured from different equipment with different calibrations, and in general may suffer from poor quality. Thus measured data may not be directly used in deriving extreme statistics. However they are used to validate the hindcast models if we are sufficiently confident with the quality of data. We now present the results of such an exercise in the context of the SEAFINE hindcast. We compared SEAFINE data (period 1956-2012) with platform measurement data from Sarawak Shell Bhd. (2008-2012).

We briefly describe the data preparation procedure before applying validation. First, we identified a common data period between the hindcast and the model (2008-2012). We then applied a standard filtering mechanism to the measured data (originally could be 10 minute intervals, averaged over 10 minutes) to make it consistent with the hindcast (60 minute intervals, averaged over 60 minutes).

Further, to compare the extremes we picked the storm peaks from the hindcast (using an approach described shortly) and chose the *corresponding* peaks from the measurements. However, we noticed that there was a slight time delay possibly due to lag in the wind field propagation. We used a simple heuristic approach to correct this and matched the peak times between the hindcast and the measurements. Storm peak significant wave height characteristics are isolated from the hindcast time-series using the procedure described in Ewans and Jonathan (2008), for a location offshore Borneo. Contiguous intervals of significant wave height above a low peak-picking threshold are identified, each interval now assumed to correspond to a storm event. The peak-picking threshold corresponds to a directional-seasonal quantile of significant wave height (H_s) with specified non-exceedance probability, estimated using quantile regression. The maximum of significant wave height during the storm interval is taken as the storm peak significant wave height. The values of directional and seasonal covariates at the time of storm peak significant wave height are referred to as storm peak values of those variables. The resulting storm peak sample consists of 262 values of H_s .

With the direction from which a storm travels expressed in degrees clockwise with respect to north, Figure 4 illustrates the storm peak identification and matching steps. Figure 4 illustrates the peaks identified using the procedure described above with the time series (grey) and peaks (black) plotted as functions of directional and seasonal covariates.

In order to effectively validate the hindcast, it is essential to compare this against a quality-controlled measured dataset belonging to a common period of interest. In particular, we are interested in comparing the peaks of the hindcast and the measurements since the extreme statistics are mostly influenced by the peaks. As mentioned earlier, directly comparing the hindcast peaks with the measurements indicated a slight time delay possibly due to the delay in the propagation of the wind field in the hindcast. This is illustrated in Figure 5 where the hindcast peaks shown in red (top) when matched with the exact time to detect the measured data peaks (middle) did not yield the actual peak. It rather resulted in measured peaks not actually being detected. It is essential to perform an appropriate comparison after correcting for this lag. We chose a relatively straightforward approach to correction. From measured peaks corresponding to a particular hindcast peak, we search in the local neighbourhood (defined by a heuristic up to 1 day window), to identify any peak which is greater than the current measured peak value. Any peak thus identified is recorded as the updated measured peak value. This is shown in Figure 5 (bottom) where the peaks are shifted appropriately, thus making it consistent with the hindcast peaks. Notice that we do not alter the value of the peaks but rather shift the peaks within the time series of measured data.

Figure 6 shows the results of a applying directional comparison between the hindcast and the measurements for a platform offshore Sarawak. Though the omni-directional scatter (left panel) does not indicate any definitive bias, observing the directional sectors we see distinct patterns. In particular, since the extreme design is driven from the north and west to some extent (owing to the stronger monsoons in those sectors), it is important to note that hindcast values appear positively biased in the north. This could possibly be due to local bathymetry inadequately represented in SEAFINE. An analysis of the actual bathymetry by the metocean team further indicated that the SEAFINE bathymetry did not account for a shallow water landmass (a shoal), just to the north of the platform. This is most likely to have caused attenuation in the wave energy before hitting the platform. Thus the hindcast is likely to show a conservative estimate especially at the northern sector.

Figure 7 show the results of a applying a seasonal comparison between the hindcast and the measurements for the platform. Here, we see a distinct apparent positive bias in the winter months (Dec - Feb), in line with the north-east monsoon as opposed to an apparent negative bias in the south-western monsoon months (July - Sep). In addition, we have developed the following tools such as the analysis of winds including directions from wind sensors, analysis of current profiles at matching depths from HYCOM2 (current hindcast), QQ plots and wind directional pdf, rosettes, etc.

In summary, we have made an earnest attempt to validate the SEAFINE hindcast by developing analysis tools and using the available measured data. Though we observed deviations between the hindcast and measured data, correction in general might be difficult. For estimating waves, the hindcast relies on regional wind field models translated to an appropriate grid with accurate bathymetry information. It is possible that the observed deviations could be due to either of them. We also compared the wind hindcast with measurements and found similar deviations. However these deviations could as well be due to inconsistencies in wind sensors (as shielding effects in the platform). Indeed for measured waves, there could also be important structural shielding effects at play. We therefore judged it prudent not to calibrate the hindcast but perform an extensive analysis across multiple sites and metocean parameters using the raw hindcast.

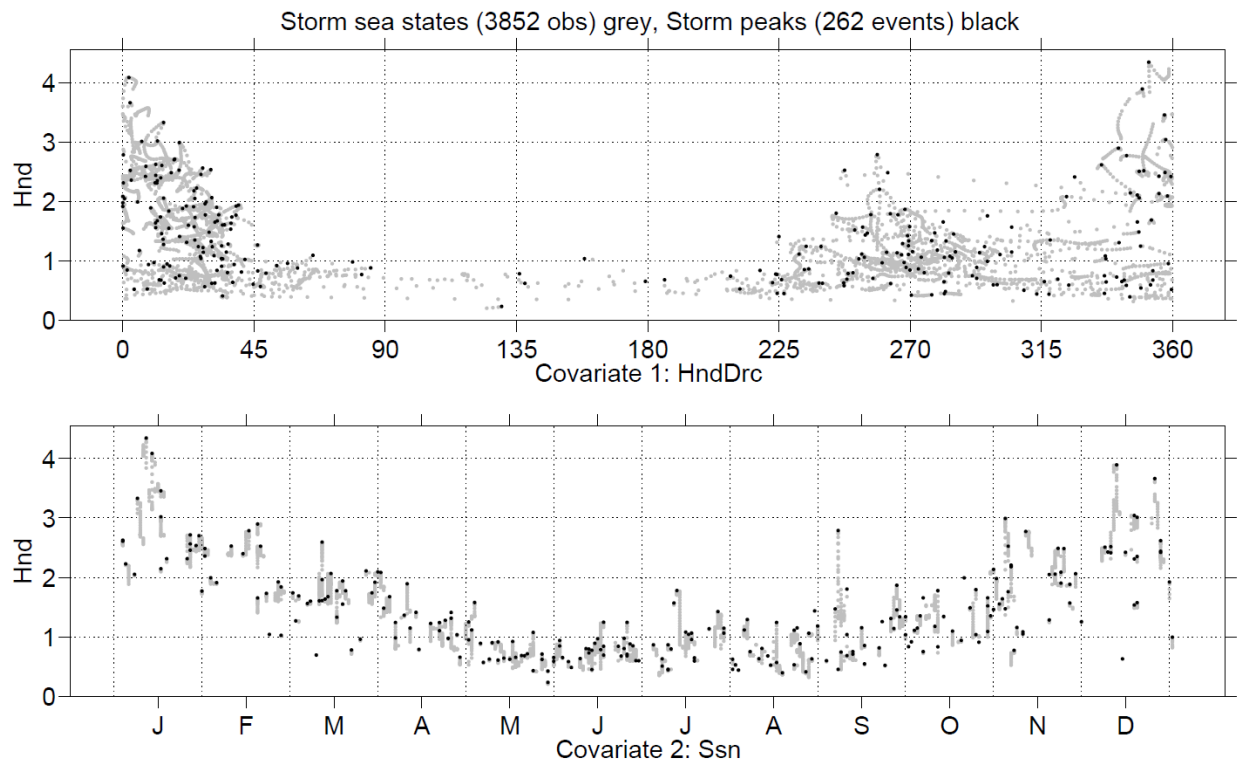


Figure 4. Data preparation for hindcast validation. Storm peak identification from hindcast time-series using a directional-seasonal threshold identification. The plots show the original hindcast time series (grey) and the peaks (black) as a function of direction (top) and season by 12 months (bottom).

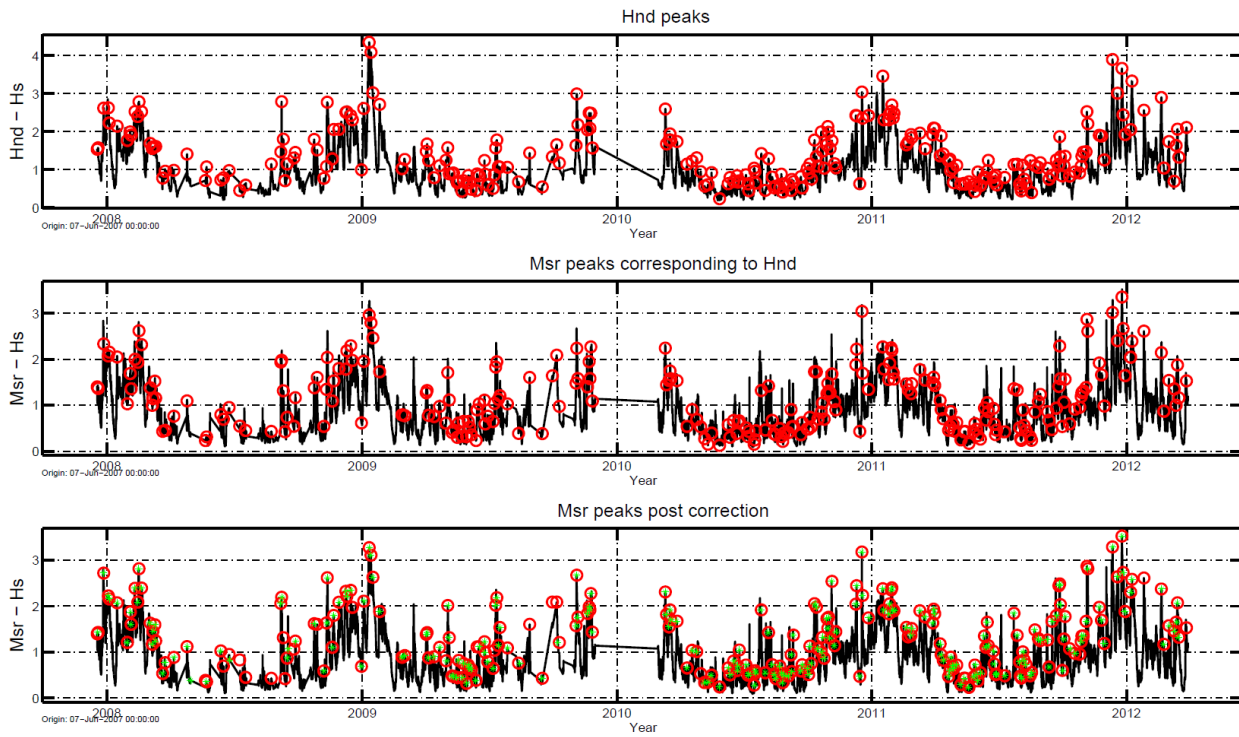


Figure 5. Data preparation for hindcast validation. Identification of corresponding storm peaks in the measured data and using a peak adjustment heuristic for the common period 2008-2012. The plots show the original hindcast time series (black) with storm peaks (red circles) of the original hindcast (top), corresponding measured data (middle), measured data with peak adjustment (bottom).

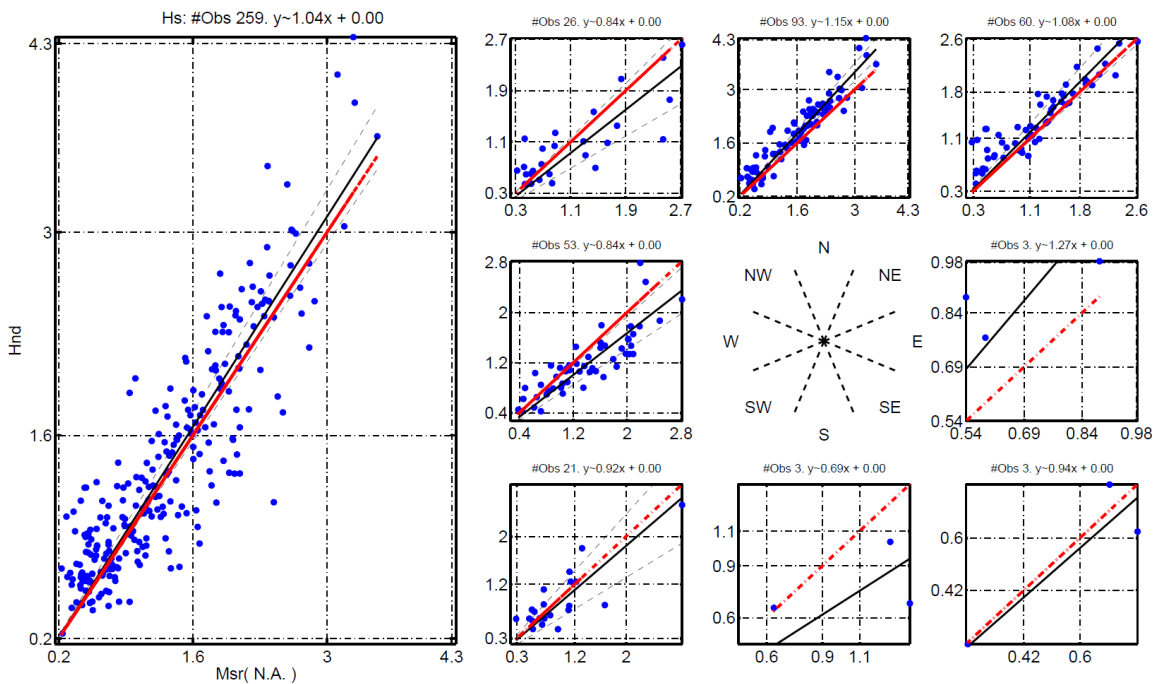


Figure 6. Validation of hindcast H_s (y -axis) against the measured (x -axis) with a *directional* scatter plot. The panels on the right show scatter comparisons for directional octants centred (from left to right, top to bottom) on NW, N, and NE; W and E; SW, S and SE respectively. Directions were those corresponding to the direction of the storm peak sea state in the hindcast data. The left panel shows the omnidirectional comparison. The black line indicates the regression fit with grey dashed showing the 95% bands and the red line indicates the slope=1 regression line. Panel titles give the number of observations followed by the regression slope coefficient. For this platform, the northern sector indicates positive bias for hindcast whereas the western sector shows a negative bias.

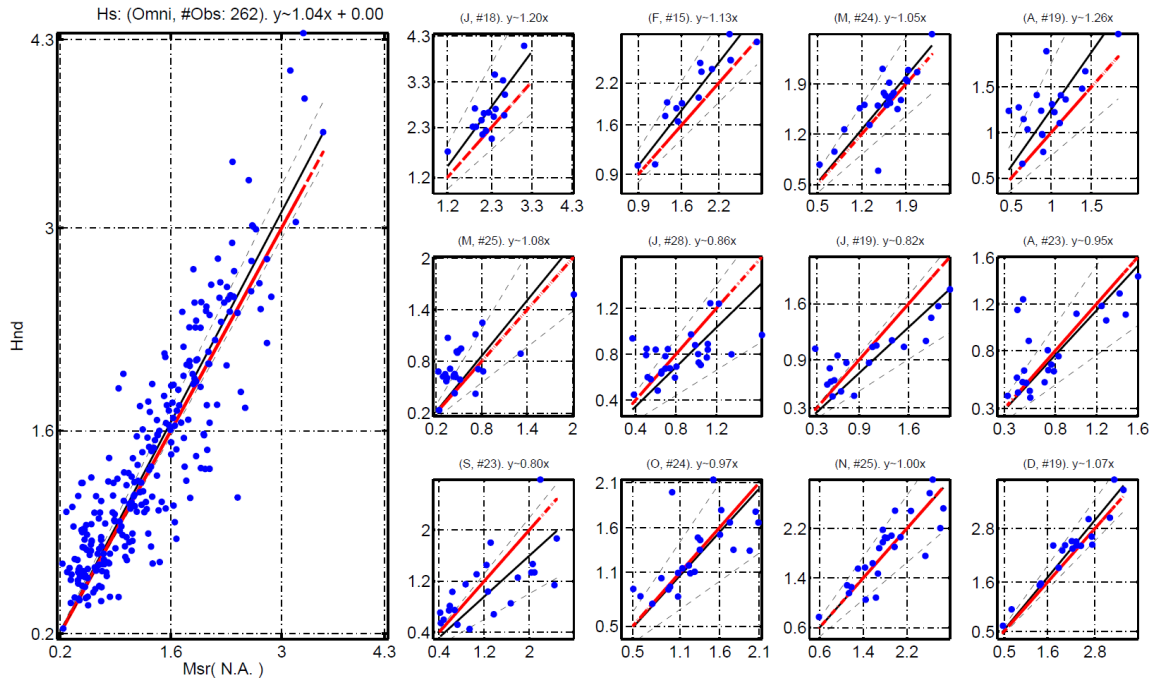


Figure 7. Validation of the hindcast H_s (y -axis) against the measured (x -axis) for the platform with a seasonal/scatter plot. The panels on the right show scatter comparisons for the 12 monthly plots (from left to right, top to bottom) respectively. The left panel shows the omni-seasonal comparison. The black line indicates the regression fit with grey dashed showing the 95% bands and the red line indicates the slope=1 regression line. Panel titles give the number of observations followed by the regression slope coefficient. For this platform, the northern hemisphere winter season (Dec-Feb) indicates positive bias for hindcast whereas in summer months (Jul-Sep) shows a negative bias.

3. Modelling

Having validated the SEAFINE hindcast and estimated the storm peaks with a spatially consistent approach, we now describe the modelling steps applied to derive extreme design criteria. The objective is the estimation of *marginal* return values for storm severity (quantified using significant wave height) for locations within a spatial neighbourhood, accounting for spatial and storm directional variability of extremal characteristics.

3.1. Model Components

Following the work of Jonathan and Ewans (2008) and Jonathan and Ewans (2011), summarised in Raghupathi et al. (2016c), we model storm peak significant wave height, namely the largest value of significant wave height observed at each location during the period of a storm event. At a given location, storm peak events are reasonably assumed to be statistically independent given covariates since they correspond to occurrences of independent atmospheric pressure fields. We assume that each storm event is observed at all locations within the neighbourhood under consideration. This is consistent with the approach considered in §2 when we propagated the peaks observed at one location across the spatial domain. Thus for a sample $\{z_i\}_{i=1}^n$ for n storm peak significant wave heights (H_s) observed at locations $\{x_i, y_i\}_{i=1}^n$ with dominant wave directions $\{\theta_i\}_{i=1}^n$ at storm peak H_s (henceforth “storm directions”), we proceed using the peaks-over-threshold approach as follows.

We first estimate a *threshold* function φ above which the observations z are assumed to be extreme. The threshold varies smoothly as a function of covariates $\varphi \triangleq \varphi(\theta, x, y)$ and is estimated using quantile regression. We retain the set of n threshold exceedances $\{z_i\}_{i=1}^n$ observed at locations $\{x_i, y_i\}_{i=1}^n$ with storm peak directions $\{\theta_i\}_{i=1}^n$ for further modelling. We next estimate the *rate* of occurrence ρ using a Poisson process model with Poisson rate $\rho \triangleq \rho(\theta, x, y)$. Finally we estimate the *size* of occurrence of

threshold exceedance using a generalised Pareto (henceforth GP) model. The GP shape and scale parameters ζ and σ are also assumed to smoothly vary as function of covariates with ζ real and $\sigma > 0$. Positivity of GP scale is ensured throughout the optimisation scheme. The GP shape parameter is unrestricted in the full optimisation, but limited to the interval $(-0.5, +0.2)$ in the estimation of the GP starting solution.

This approach to extreme value modelling follows that of Chavez-Demoulin and Davison (2005) and is equivalent to direct estimation of a non-homogeneous Poisson point process model (Dixon et al. (1998), Jonathan and Ewans (2013)). We emphasise that, in common with Chavez-Demoulin and Davison (2005) and Jonathan and Ewans (2013), we perform marginal non-stationary extreme value analysis across a grid of (dependent) spatial locations, accounting (per location) for directional and spatial variability in extremal characteristics. We further account for the effects of (extremal) spatial dependence between locations on inferences using a block bootstrapping scheme.

3.2. Parameterising Covariates

Applying the model to whole-basin applications is methodologically straightforward, but computationally challenging. Physical considerations suggest we should consider parameters φ , ρ , ξ and σ to be smooth functions of covariates θ, x, y (Randell et al., 2013). For estimation, this can be achieved by expressing the value of each parameter in terms of a linear combination of appropriate basis for the domain D of covariates, where $D = D_\theta \times D_x \times D_y$. Here $D_\theta = [0, 360)$ is the (marginal) domain of storm peak directions, and D_x, D_y are the domains of x - and y -values (e.g. longitudes and latitudes) under consideration.

For each covariate (and marginal domain) in turn, we first calculate a B-spline basis matrix for an index set of size m ($m \ll n$) of covariate values; potentially we could calculate the basis matrix for each of the n observations, but usually avoid this for computational and statistical efficiency. For instance in the case of D_θ , we calculate an $m_\theta \times p_\theta$ basis matrix B_θ such that the value of any function at each of the m_θ points in the index set for storm direction can be expressed as linear combination $B_\theta \beta_\theta$ for some $p_\theta \times 1$ vector β_θ of basis coefficients. Note that periodic marginal bases can be specified if appropriate (e.g. for D_θ).

Then we define a basis matrix for the three-dimensional domain B using tensor products of marginal basis matrices. Thus

$$B = B_y \times B_x \times B_\theta$$

provides an $m \times p$ basis matrix (where $m = m_\theta m_x m_y$, and $p = p_\theta p_x p_y$) for modelling each of φ , ρ , ξ and σ on the corresponding ‘‘spatio-directional’’ index set of size m . Any φ , ρ , ξ and σ (η , say, for brevity) can then be expressed in the form $\eta = B\beta$ for some $p \times 1$ vector β of basis coefficients. Model estimation therefore reduces to estimating appropriate sets of basis coefficients for each of φ , ρ , ξ and σ .

The value of any marginal p_i (i.e. p_θ , p_x or p_y) is equal to the number q_i of spline knots specified for periodic domains (e.g. for D_θ), and to $q_i + d_i$ for aperiodic domains (e.g. for D_x and D_y), where d_i is the order of the B-spline function specified (always 3 in this work, so that spline functions are twice differentiable).

The roughness R of any function η defined on the support of the spline basis can be easily evaluated on the index set (at which $\eta = B\beta$). For a one-dimensional (e.g. directional) spline basis, following the

approach of Eilers and Marx (2010), writing the vector of differences of consecutive values of β as $\Delta\beta$, and vectors of second and higher order differences using $\Delta^k\beta = \Delta(\Delta^{k-1}\beta)$, $k=2,3, \dots$ the roughness R of η is given by

$$R = \beta' P \beta$$

where $P = (\Delta^k)'(\Delta^k)$ for differences of order k (with appropriate modifications to preserve periodicity as necessary). For a spatio-directional spline basis, the penalty matrix P can be similarly defined using

$$P = P_y \times P_x \times P_\theta$$

in the obvious notation. We use $k=1$ throughout this work. With this choice of k , heavy roughness penalisation results in stationarity of parameters with respect to periodic and aperiodic covariates. To avoid potential over-fitting, parameter estimation requires that the (negative log) likelihood function is penalised using a linear combination of parameter roughnesses with roughness coefficients λ_η (for each model parameter η). The choice of optimal penalty coefficients is determined by block cross-validation, further adding to computational complexity. Since each storm is observed as a spatially-dependent event at all spatial locations, we define a storm ‘‘block’’ to be the set of occurrences of a particular storm at all locations for the purposes of both cross-validation (in estimation of model smoothness) and bootstrapping (for uncertainty quantification). For the spatio-directional problem, it is also possible to vary the relative size of basis penalisation with respect to direction, longitude and latitude. In this work, the same penalty value was adopted for both spatial co-ordinates, and the relative value of the directional to spatial penalty was decided using a series of experiments with different penalty choices. We manage the considerable computational challenges of basin-wide extreme value modelling using a combination of generalised linear array methods (GLAM) and parallel computing as described in Raghupathi et al. (2016c).

4. Large Scale Extremes Model: Results

4.1. Spatio-directional Model

We now present the results of applying the spatio-directional model described in §3 to the SEAFINE data after validating and applying the peak picking algorithm of §2. First, in Figure 8 we show the approximate location of the spatial grid offshore Sarawak with a resolution of 0.1 degrees. This is the subset of the spatial grid from the SEAFINE hindcast described in §2.2 that has been used for analysis throughout this section. Second, we validate the hindcast with measurements from known location within this grid using the technique described in §2.4. Finally, we generate the exact set of peaks from the spatial peak picking procedure described in §2.3. From the spatial peaks thus generated, we apply the spatio-directional extreme value model described in §3 first by estimating model parameters for threshold, rate of occurrence followed by the generalised Pareto shape and scale. Following a sensitivity study into the stability of GP shape parameter and median 100-year return value with threshold non-exceedance probability, a threshold non-exceedance probability of 0.8 was deemed appropriate.

Figure 9 (a) shows marginal plots of threshold against direction, longitude and latitude. The highest thresholds can be seen for storms from the north which is consistent with raw data. The threshold values are higher for smaller longitudes and higher latitudes (i.e., north-west grid locations towards the open oceans) which is consistent with the physical phenomena. Figure 9 (b) shows the marginal plots of the rate of occurrence against direction, longitude and latitude. The rate of occurrence is relatively similar for all longitude and latitude but for events in the northern ($330^\circ - 45^\circ$) and the western ($250^\circ - 290^\circ$)

directional sectors. This is consistent with the directional effects of the north-east and south-west monsoon. Figure 9 (c) shows marginal plots of the GP shape and scale against direction, longitude and latitude. The GP shape is relatively similar for all directions, longitude and latitude. The GP scale has larger values for lower longitude (east) and higher latitude (north).

Figure 10 shows the model parameter estimates as functions of spatio-directional covariates, spatially for directional octants and for all directions (or “omni-directionally”). Note that the units for parameters are as follows: threshold (metres), rate of threshold exceedance (occurrences per degree per location per annum), GP shape (dimensionless) and GP scale (metres). The threshold estimate is relatively stable with respect to both space and direction at around 2m except the northern sectors where the strongest winds occur (primarily due to north-east monsoon and winter typhoons) suggesting that extreme values in this region will be larger than elsewhere. The northern sector threshold also reflects the increasing intensity in storm severity towards the northeast. The rate of occurrence of threshold exceedances is highest for storms from the north and north-east as expected from physical considerations. Though the GP shape appears to be almost constant, locations in the north-eastern region exhibit larger GP scale, suggesting that extreme values in this region will be larger than elsewhere (mostly due to those regions belonging to deeper waters) - again consistent with historical evidence. Estimated values of GP shape is around -0.1 and GP scale varies from 0.40 to 0.65. Maximum likelihood estimators for GP shape and scale are asymptotically negatively dependent and it is common in applications to observe negative dependence between estimates of these parameters (see, e.g., Scarrott and MacDonald (2012)).

Model diagnostics are essential to demonstrate adequate model fit. Of primary concern is that the estimated extreme value model generates spatio-directional distributions consistent with observed storm peak data (see Feld et al. (2015), Jonathan et al. (2014)). Figure 11(a) provides a spatial comparison of cumulative distribution functions for return values for the period of the original sample, estimated using the original sample (red) and using 1000 realisations under the model (black) for a 3 x 3 grid of locations around the SCS, which is the current interest. Figure 11(b) gives the corresponding directional comparison. There is good agreement. Wider uncertainty bands in southern and south-western directional sectors are due to lower rates of occurrence of hurricanes.

Return value distributions can be estimated by the simulation procedure described in Jonathan et al. (2014). Briefly, for each location in turn, the distribution of the 100-year return period is estimated omni-directionally and for 8 directional sectors of equal size centred on cardinal and semi cardinal directions, using all of the estimated extreme value models (for the actual sample and its bootstrap resamples). Figure 12 shows median 100-year marginal return values for the spatial grid shown in Figure 8, incorporating directional dissipation (as described in Jonathan et al. (2014)). Omnidirectional estimates (lower panel) of approximately 5-6m are consistent with expectation. Directionally, the most severe storms occur in the northern and north-eastern sectors, consistent with physical understanding. Largest return values occur in the north-eastern region towards the open sea. Using model output such as that in the figure, the metocean specialist can access extreme value estimates for any spatial location and directional octant of choice, generated by a thorough consistent approach for the whole ocean basin.

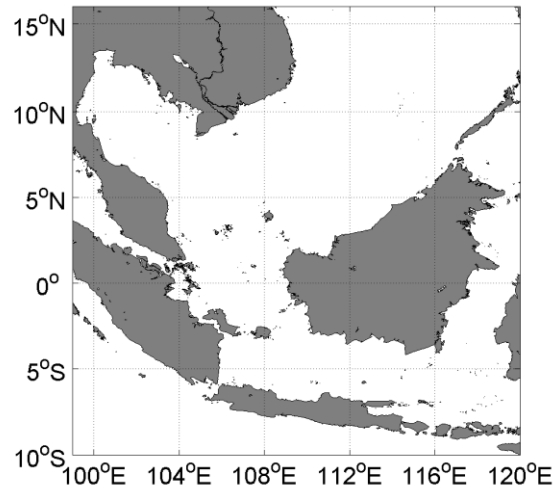


Figure 8. The geography of the South China Sea. Our grid of locations is offshore Sarawak at approximately 112° E, 5° N.

4.2. Spatio-directional and direction-only model comparison

Recall that the main objective of this work is to derive spatially-consistent design criteria for the SCS locations. The results above have indeed met that objective. Thus for a practicing engineer who is interested in deriving criteria for a single site, the spatial model can easily provide design inputs. However it is useful to demonstrate that model fits from a spatio-directional model (proposed approach) and a site-specific directional model (current best in class practice) are comparable. Figure 13 compares the model diagnostics for a given platform location derived from a spatio-directional model (top) and a site-specific model (below) using the following procedure.

We use a return value simulation similar to those discussed in the previous section to assess model adequacy. Specifically, we simulate multiple realisations of sets of sea-state H_s events corresponding exactly to the period of the original sample under the model. For each set simulated, we construct a cumulative distribution function (actually, $1 - \log(\text{cdf})$ to emphasise tail behaviour), potentially restricted to some co-variate interval A , and estimate 2.5% and 97.5% values of the cdf for each value of H_s . These curves, with 95% confidence intervals, are illustrated in dashed grey and the median in solid grey is compared with the median cumulative distribution function for the original sample, illustrated in red in the figure. Two sets of plots are generated one each for spatio-directional model (top) and a site-specific model (bottom). Agreement is good for omni-directional and sectoral estimates shown for H_s . We thus can be satisfied that the SCEVA model is comparable to the site-specific model for the sites of interest. We expect the estimates using the spatio-directional model to be better than from the site-specific directional model. The size of the confidence limits appears to support that view. Therefore given a set of spatial locations, our spatial model may be used to generate consistent set of design criteria for all the points in the region.

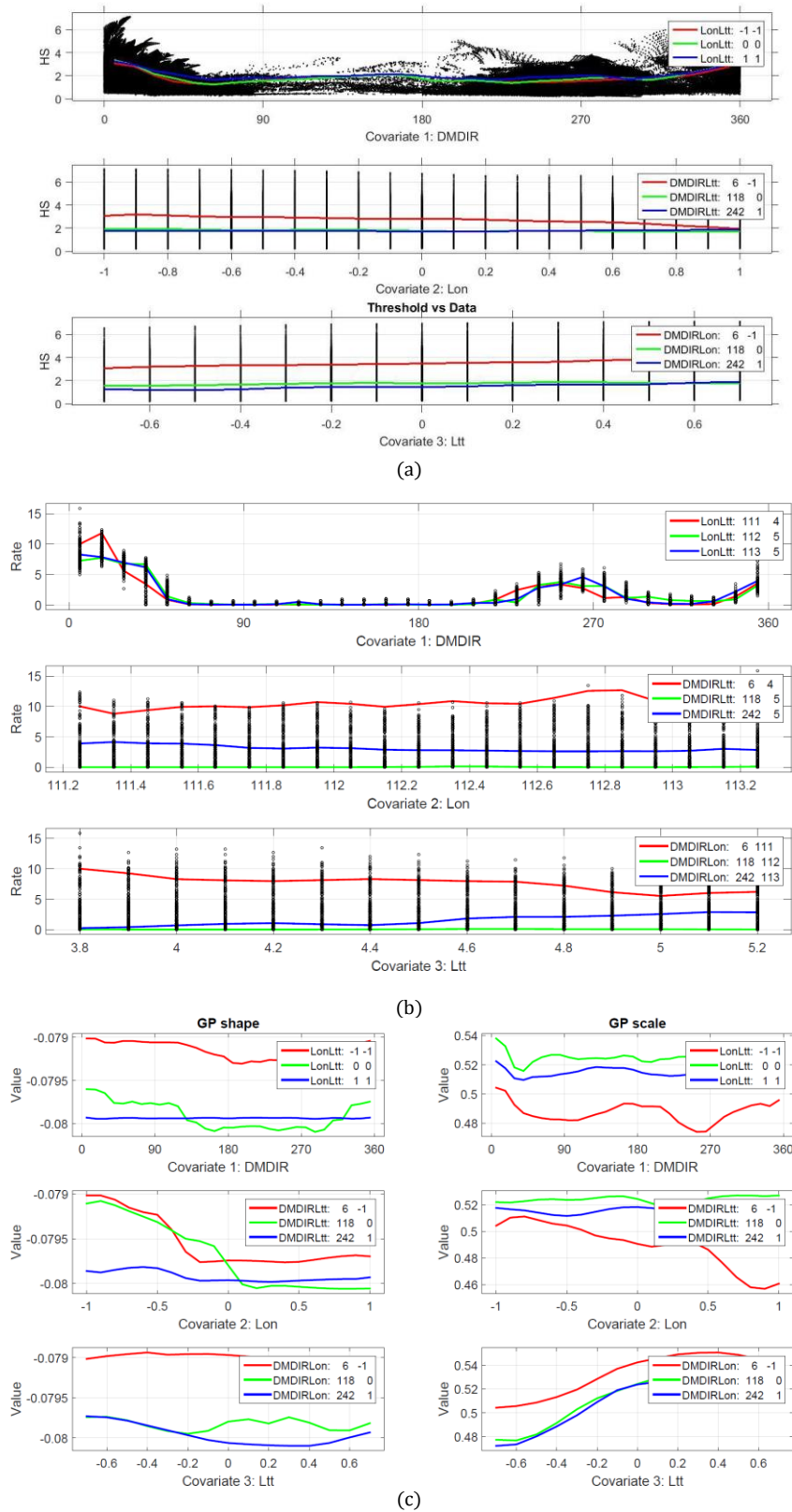


Figure 9. Model parameter estimates for the spatial grid in the SCS: (a) threshold (metres), (b) rate of threshold exceedance (occurrences per degree per spatial location per annum), (c) GP shape (dimensionless) and scale (metres). In each panel, the upper plot gives parameter estimates as a function of direction for typical SW (red), centre (green) and NE (blue) locations respectively; the middle plot as a function of longitude for storms from 0° and minimum latitude (red), from 120° and central latitude (green) and 240° and maximum latitude (blue); the bottom plot as a function of latitude for storms from 0° and minimum longitude (red), from 120° and central longitude (green) and from 270° and maximum longitude (blue).

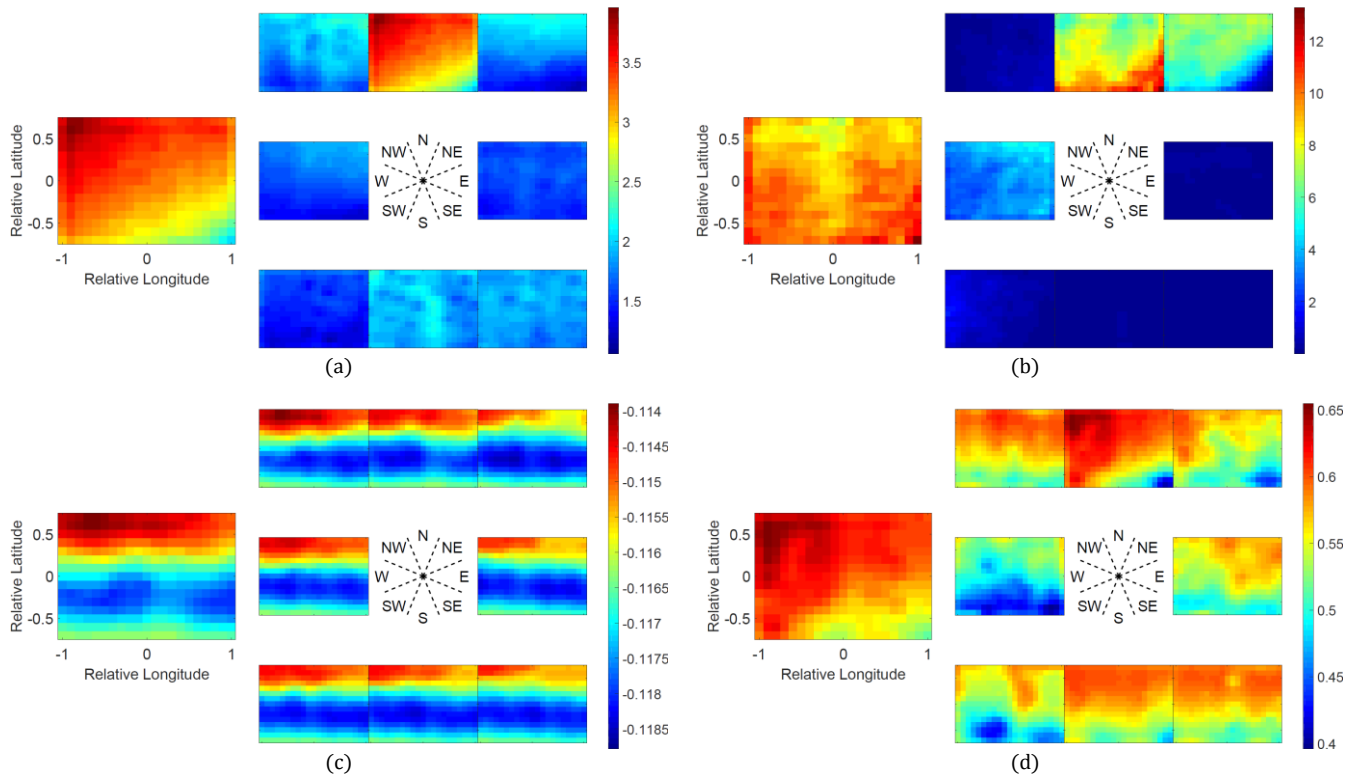


Figure 10. Spatio-directional plot of the model parameter estimates for the spatial grid in the SCS: (a) threshold (metres), (b) rate of threshold exceedance (occurrences per degree per spatial location per annum), (c) GP shape (dimensionless) and (d) scale (metres). For each parameter, the lower plot shows median omnidirectional parameter estimates for each of 315 locations. The 8 upper plots show median directional sector parameter estimates per location for 8 directional octants centred (from left to right, top to bottom) on storms from NW, N, and NE; W and E; SW, S and SE respectively.

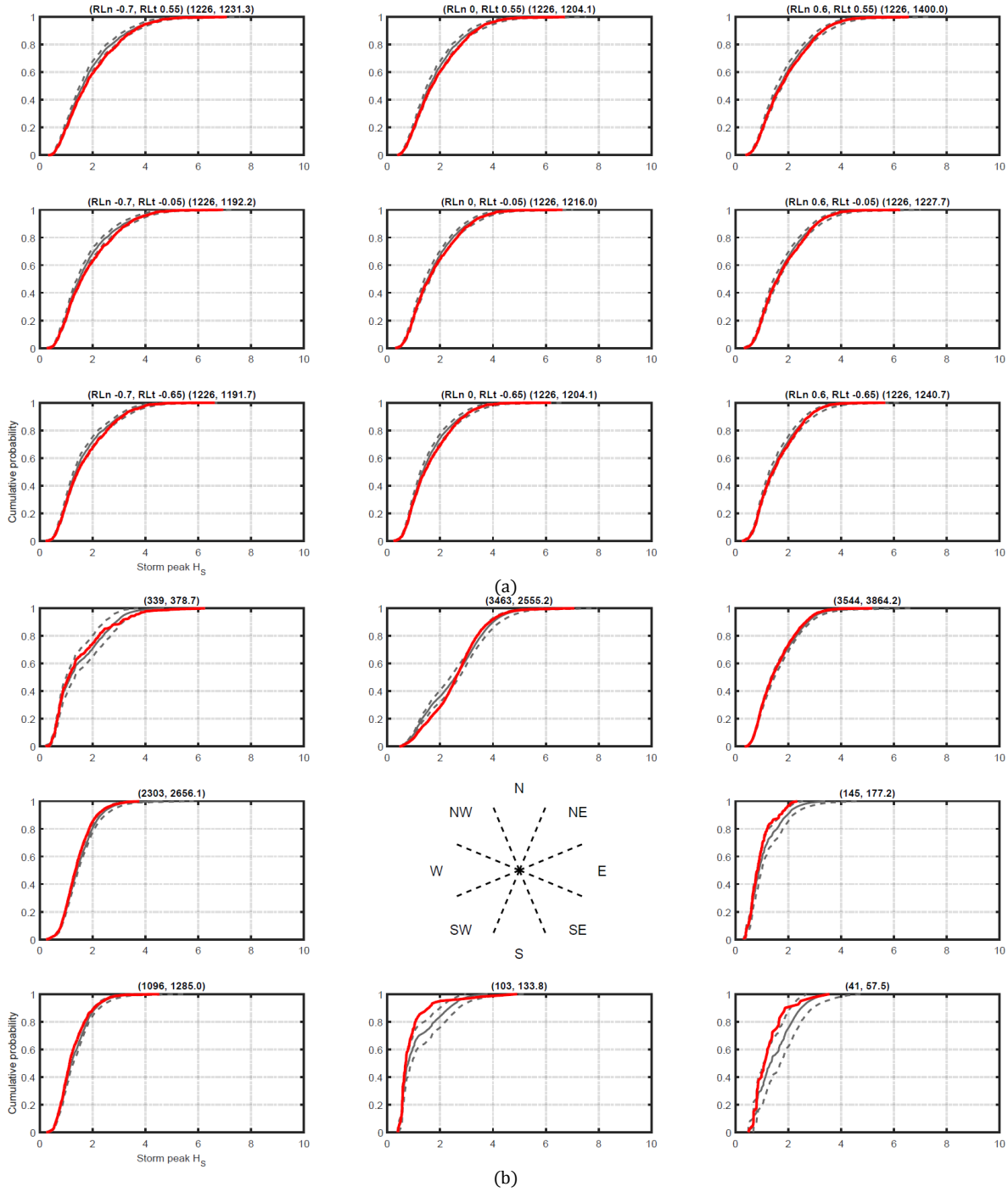


Figure 11.: Validation of the spatio-directional model by (a) spatial and (b) directional comparison of cumulative distribution functions (cdf) for return value distributions of the original sample (red) with those from 1000 realisations under the model corresponding to the same time period as the original sample, shown in terms of the median (solid grey) and 95% uncertainty band (dashed grey). Figure (a) corresponds to omnidirectional comparisons for a 3 x 3 grid of locations in the spatial domain, the relative longitudes and latitudes of which are given in the panel titles. The second pair of numbers in the panel title gives the number of observed and (average) simulated observations. Figure (b) gives a comparison of distributions for directional octants (for the same 3 x 3 grid of locations) centred (from left to right, top to bottom) on NW, N, and NE; W and E; SW, S and SE respectively. Panel titles give the number of observed and (average) simulated observations. Return values are measured in metres.

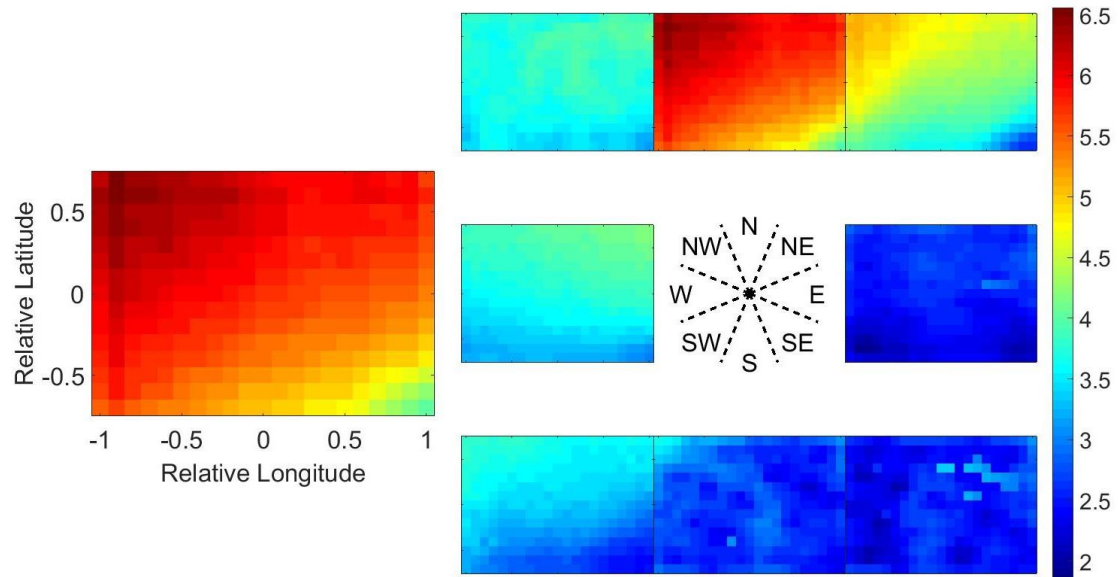


Figure 12. Spatio-directional plots for the median of the 100-year return value distribution for the spatial grid in SCS. In each figure, the lower panel shows the omnidirectional estimate per location, and the 8 upper panels show estimates per directional sector per location for 8 directional octants centred (from left to right, top to bottom) on storms from NW, N, and NE; W and E; SW, S and SE respectively. The common colour scale is in metres.

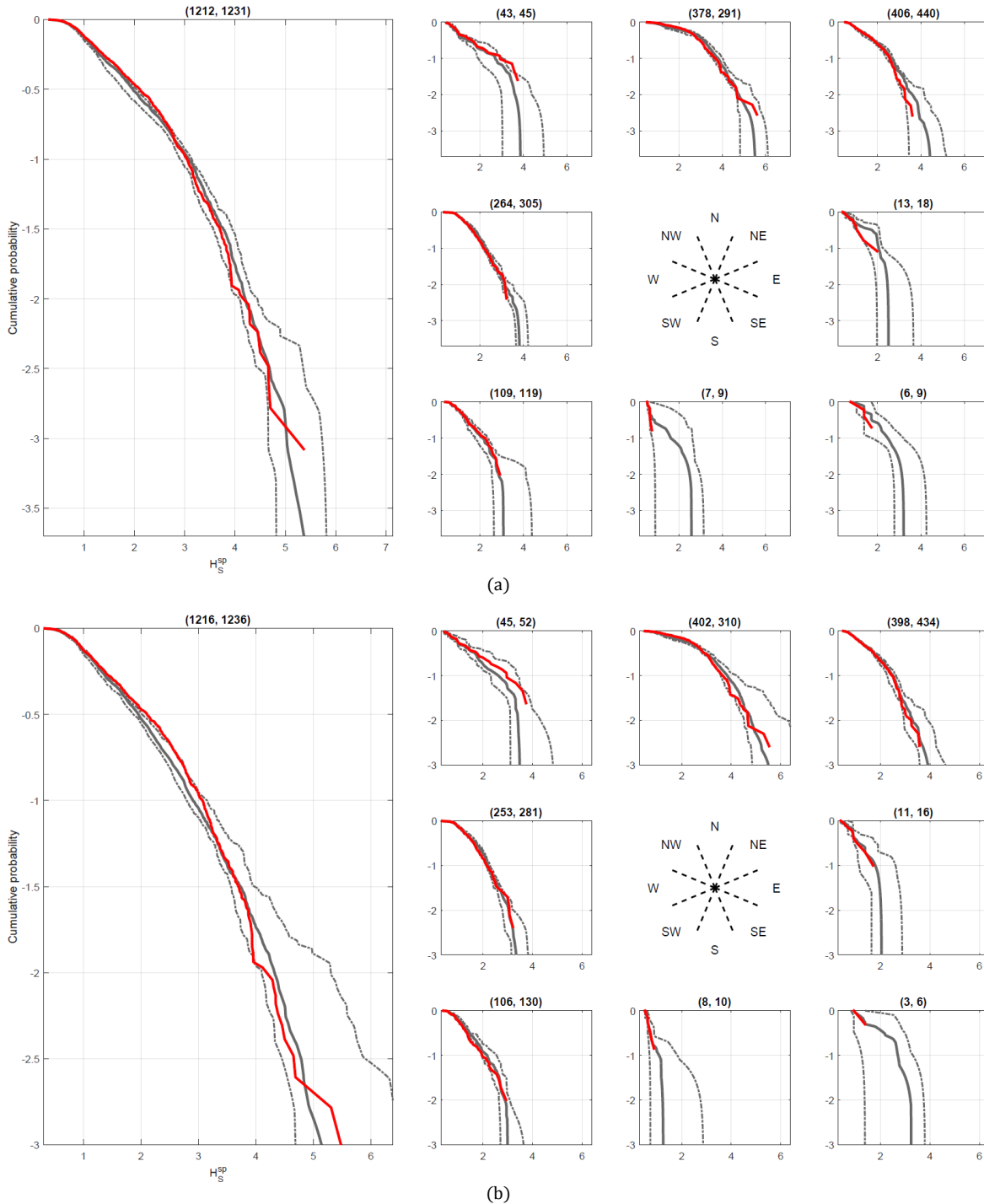


Figure 13. Comparison of model diagnostics generated for a specific site between a (a) spatio-directional model for the *whole* grid that also includes the same site and (b) a directional model fitted *only* for that exact site. Each plot shows the comparison of cumulative distribution functions ($1 - \log(\text{cdf})$) to emphasise tail behaviour) for return value distributions of the original sample (red) with those from 1000 realisations under the model corresponding to the same time period as the original sample, shown in terms of the median (solid grey) and 95% uncertainty band (dashed grey). For each plot, the 8 right hand panels show the cdf comparisons per directional sector for the 8 directional octants centred (from left to right, top to bottom) on NW, N, and NE; W and E; SW, S and SE respectively. The left-hand panel shows the equivalent omnidirectional comparison. Return values are measured in metres. The title in each panel (in parenthesis) gives the number of observed and (average) simulated observations.

5. Discussion & Conclusions

Metocean engineers often need to analyse large amount of data for different sites in order to estimate design criteria. This can often lead to inconsistent application of design procedures and inconsistent design estimates. In addition, the activity is often laborious and repetitive. Our objective is to provide rational and consistent design estimates using high-quality data with best in class statistical tool using **Spatial Covariate Extreme Value Analysis (or SCEVA)**. We overcame several technical challenges to produce spatially-consistent independent marginal design criteria for locations in the South China Sea using the high-resolution SEAFINE database. Most notably, we successfully validate the proposed spatio-directional model by comparing its diagnostics to a site-specific directional model. The advantage of a *single* model that adequately characterises spatial and directional effects is obvious. Not only do we get spatially-consistent design, such that neighbouring locations have similar extreme value characteristics, but we also avoid the need for repetitive site-specific analysis, and we expect improved reliability of the extremal estimates for a specific site (by comparison with a non-spatial model) due the inclusion of data from surrounding grid points in the estimate. To our knowledge, this is the first time that such an endeavour has been attempted for the SCS region.

There are considerable opportunities for application and further development of this approach. The current work addresses extreme value modelling of one variate (e.g. storm peak H_s) conditional on multidimensional covariates (e.g. space-direction). Other recent work (e.g. Raghupathi et al. (2016b)) has outlined how the method can be extended to the conditional modelling of one variate (e.g. storm peak current speed) given extreme values of another (e.g. storm peak H_s) and one or more covariates (e.g. current direction, storm direction and season). Further, spatial dependence models (e.g. Davison et al. (2012)) seek to characterise extremal spatial dependence across multiple locations as well as marginal non-stationarity.

Incorporating seasonal effects could be an another area of potential application though in case of the South China Sea there appears to be a direct correlation between directional and seasonal effects (Randell et al., 2015a). However it would be worthwhile to establish such a model in the spatial context to actually see the full relationship. This would necessitate the establishment of a four-dimensional spatio-directional-seasonal model parameterisation. This would also mean that the different smoothness of the spline basis would have to adjust to different dimensions. A robust estimation of the spline parameters could possibly be attempted through the extension of the recently proposed Bayesian inference (Randell et al., 2015b), which appears to offer yet further computational advantages. The validation approach shown here for hindcast values with respect to measurements needs to be extended and an appropriate calibration strategy formulated. This may be challenging in general, but any valid approach must accommodate uncertainties in both measured and hindcast values in achieving a realistic hindcast calibration.

Acknowledgements

We are thankful to the support and encouragement of Vianney Koelman and Bertwim van Beest from the Computational Technology Platform, metocean engineers Graham Feld, Fan Shejun and Vadim Anokhin, useful discussions with team members in Bangalore, Kuala Lumpur, Miri and Manchester, and academic colleagues at Lancaster University.

References

- Borneo (2015). Borneo Weather. <http://www.borneo.com.au/general/weather>. Accessed: 2015-11-3.
- Chavez-Demoulin, V. and Davison, A. (2005). Generalized Additive Modelling of Sample Extremes. *J. Roy. Statist. Soc. Series C: Applied Statistics*, 54:207.
- Davison, A. C., Padoan, S. A., and Ribatet, M. (2012). Statistical Modelling of Spatial Extremes. *Statistical Science*, 27:161-186.
- Dixon, J. M., Tawn, J. A., and Vassie, J. M. (1998). Spatial Modelling of Extreme Sea-levels. *Environmetrics*, 9:283-301.
- Eilers, P. H. C. and Marx, B. D. (2010). Splines, Knots and Penalties. *Wiley Interscience Reviews: Computational Statistics*, 2:637-653.
- Ewans, K. C. and Jonathan, P. (2008). The Effect of Directionality on Northern North Sea Extreme Wave Design Criteria. *J. Offshore Mech. Arc. Engg.*, 130(10).
- Feld, G., Randell, D., Wu, Y., Ewans, K., and Jonathan, P. (2015). Estimation of Storm Peak and Intra-storm Directional-seasonal Design Conditions in the North Sea. *J. Offshore. Arct. Eng.*, 137:021102:1-15.
- Jonathan, P. and Ewans, K. C. (2008). On Modelling Seasonality of Extreme Waves. In *Proc. 27th International Conf. on Offshore Mechanics and Arctic Engineering, 4-8 June, Estoril, Portugal*.
- Jonathan, P. and Ewans, K. C. (2011). A Spatiodirectional Model for Extreme Waves in the Gulf of Mexico. *ASME J. Offshore Mech. Arct. Eng.*, 133:011601.
- Jonathan, P. and Ewans, K. C. (2013). Statistical Modelling of Extreme Ocean Environments with Implications for Marine Design: A Review. *Ocean Engineering*, 62:91-109.
- Jonathan, P., Randell, D., Wu, Y., and Ewans, K. (2014). Return Level Estimation from Nonstationary Spatial Data Exhibiting Multidimensional Covariate Effects. *Ocean Eng.*, 88:520-532.
- Oceanweather (1992). SEAMOS: South East Asia Meteorological and Oceanographic Study. <http://www.oceanweather.com/metocean/seamos/>. Accessed: 2015-10-19.
- Oceanweather (2008). GOMOS08: Gulf of Mexico Oceanographic Study. <http://www.oceanweather.com/metocean/gomos/index.html/>. Accessed: 2015-10-19.
- Oceanweather (2014). SEAFINE: SEAMOS South FINEgrid Hindcast Study. <http://www.oceanweather.com/metocean/seafine/>. Accessed: 2015-10-19.
- Raghupathi, L., Jonathan, P., and Ewans, K. (2016a). Spatial Identification of Storm Peaks for Large Scale Extreme Value Analysis. In *Under preparation*.
- Raghupathi, L., Randell, D., Ewans, K., and Jonathan, P. (2016b). Non-stationary Estimation of Joint Design Criteria with a Multivariate Conditional Extremes Approach. In *Under preparation*.
- Raghupathi, L., Randell, D., Jonathan, P., and Ewans, K. (2016c). Fast Computation of Large Scale Marginal Spatio-Directional Extremes. *Comp. Stat. Dat. Anal.*, 95:243-258.
- Randell, D., Feld, G., Ewans, K. C., and Jonathan, P. (2015a). Distributions of Return Values for Ocean Wave Characteristics in the South China Sea using Directional-seasonal Extreme Value Analysis. *Environmetrics*, 26(6):442-450.
- Randell, D., Turnbull, K., Ewans, K., and Jonathan, P. (2015b). Bayesian Inference for Nonstationary Marginal Extremes. *Environmetrics*, Submitted.
- Randell, D., Yu, Y., Jonathan, P., and Ewans, K. C. (2013). Modelling Covariate Effects in Extremes of Storm Severity on the Australian North West Shelf. In *Proc. 32nd Intl. Conf. Offshore Mech. Arc. Eng., Nantes, France*.
- Scarrott, C. and MacDonald, A. (2012). A Review of Extreme Value Threshold Estimation and Uncertainty Quantification. *Revstat*, 10:33-60.